Biosensors and Bioelectronics 223 (2023) 115018

Contents lists available at ScienceDirect

Biosensors and Bioelectronics

journal homepage: www.elsevier.com/locate/bios

Wireless, AI-enabled wearable thermal comfort sensor for energy-efficient, human-in-the-loop control of indoor temperature

Seonghun Cho [a], Hong Jae Nam [a], Chuanqi Shi [b], Choong Yeon Kim [a], Sang-Hyuk Byun [a], Karen-Christian Agno [a], Byung Chul Lee [c], Jianliang Xiao [b], Joo Yong Sim [d,**], Jae-Woong Jeong [a,e,*]

[a] School of Electrical Engineering, Korea Advanced Institute of Science and Technology (KAIST), Daejeon, 34141, South Korea
[b] Department of Mechanical Engineering, University of Colorado Boulder, Boulder, CO, 80309, USA
[c] Bionics Research Center, Korea Institute of Science and Technology (KIST), Seoul, 02792, South Korea
[d] Department of Mechanical Systems Engineering, Sookmyung Women's University, Seoul, 04310, South Korea
[e] KAIST Institute for Health Science and Technology, Korea Advanced Institute of Science and Technology (KAIST), Daejeon, 34141, South Korea

ARTICLE INFO

Keywords:
Thermal comfort
Human-in-the-loop
Wearable sensor
Temperature sensor
Artificial intelligence
Energy saving

ABSTRACT

The conventional heating, ventilation, and air conditioning (HVAC) systems are based on a set-point control approach that only considers the temperature of the environment without reflecting the thermophysiological status of the occupant. This approach not only fails to fully satisfy individual thermal preferences, but it also makes an HVAC operation energy-inefficient. One possible solution is to control the indoor thermal condition based on an accurate prediction of the occupant's thermal comfort to prevent any unnecessary energy consumption. Here, we present an artificial intelligence (AI) wearable sensor-based human-in-the-loop HVAC control system that is operated on a real-time basis reflecting the thermophysiological condition of the occupant to automatically improve their thermal comfort while reducing the energy consumption of the building. The wristband-type, AI-based, three-point wearable temperature sensor offers excellent thermal comfort prediction accuracy (93.9%), enabling a human-centric HVAC control operation. A proof-of-concept demonstration of closed human-in-the-loop HVAC control using the AI-enabled wearable sensor system confirms both the accuracy of the thermal comfort prediction and the energy-efficiency of this approach, demonstrating its potential as a new solution that improves the occupant's thermal comfort and provides building energy savings.

1. Introduction

The continuous increase in energy consumption worldwide, with estimated growth of about 50% by 2050, is a serious problem as it requires burning of more fossil fuels which accounts for two-thirds of greenhouse gas emissions (Damassa, 2014; van Ruijven et al., 2019). The structural building energy demand constitutes 35% of the total global energy demand, and heating, ventilation, and air conditioning (HVAC) systems are one of the major contributors to this, accounting for about 50% of the total energy demand in buildings (Nalley and LaRose, 2021). Existing HVAC systems use a set-point control method with indoor temperature sensors to control the thermal environment of the area for human comfort. However, this approach is not optimal since it only considers the temperature of the environment and does not include the individual's preferences for the thermal environment. This not only can increase the power consumption but also can reduce the thermal comfort of the occupants (Han et al., 2019; Hu et al., 2020; Peng and Cui, 2020). Previous reports pointed out a direct relationship of thermal comfort of the occupants to their productivity (Akimoto et al., 2010; Collinge et al., 2014), indicating the importance of thermal comfort of workers in office buildings.

Recent thermal comfort prediction technologies based on artificial intelligence (AI) have been shown to improve thermal comfort, with potential application for building energy savings as well. Prediction approaches, such as supervised learning with various regression and classification models (Cosma and Simha, 2019; Katić et al., 2020; Morresi et al., 2021), as well as reinforcement learning (Gao et al., 2020; Valladares et al., 2019), have been conducted to achieve optimal

* Corresponding author. School of Electrical Engineering, Korea Advanced Institute of Science and Technology (KAIST), Daejeon, 34141, South Korea.
** Corresponding author.
E-mail addresses: jysim@sookmyung.ac.kr (J.Y. Sim), jjeong1@kaist.ac.kr (J.-W. Jeong).

https://doi.org/10.1016/j.bios.2022.115018
Received 16 August 2022; Received in revised form 7 December 2022; Accepted 15 December 2022
Available online 17 December 2022
0956-5663/© 2022 Elsevier B.V. All rights reserved.

thermal comfort control. However, these studies have not yet been verified in a closed human-in-the-loop (HIL) with an HVAC control system. Previous alternative control simulations based on the dataset of the American Society of Heating, Refrigerating and Air-Conditioning Engineers (ASHRAE RP-884), which is composed of thermal comfort field experiments carried out worldwide (21,000 samples from 160 buildings), were evaluated in terms of their performance in an integrated HIL-HVAC control system, but the physiological data (e.g., skin temperature, sweat rate), which play a major role in thermoregulation (Fang et al., 2021), were not included in the data training (Gao et al., 2020; Kramer et al., 2021). A recent field study (Li et al., 2021) utilized physiological sensing technologies (e.g., skin temperature, heart rate, etc.) using a commercial wristband for thermal comfort prediction and optimal control of an HVAC system. A linear-regression-model-based method was used in the study to update the thermal sensation prediction model in real time. Nonetheless, commercial wristband sensors have limited thermal comfort prediction accuracies, as they do not allow variation of different numbers and locations of skin temperature measurements.

In this work, we introduce an AI-enabled HIL-HVAC wearable sensor control system with real-time, thermophysiological condition-dependent operation, which can automatically enhance the thermal comfort of the occupant with potential to reduce the energy consumption of the building. Among the various physiological measures that are typically used in predicting human thermal comfort (e.g., sweat rate (Sim et al., 2018), blood pressure (Charkoudian, 2003), skin temperature (Choi and Loftness, 2012)), we adopted the skin temperature as a key physiological measure, owing to its important role in thermal transfer according to thermal comfort theory (Romanovsky, 2014), as well as the ease of reducing the overall dimensions of devices operated with thermal sensors (Mansi et al., 2021). Here, we developed a soft wearable sensor, which offers a real-time, three-point wrist skin temperature measurement that has potential to improve the prediction accuracy of the thermal comfort as compared with a single-point measurement (Sim et al., 2016). Using the three-point temperature measurement, our optimal thermal comfort prediction model shows 93.9% accuracy, as compared with the conventional single-point temperature measurement using a commercial temperature sensor with accuracy of 87% (Chaudhuri et al., 2018a). Real-time temperature detection of the wearable sensor is possible owing to its wireless linkage to an AI-based HVAC control system that regulates the indoor temperature. Finally, our system demonstration exhibits an optimized HIL-HVAC control operation according to the occupant's thermal comfort status that substantially reduces the energy consumption by 20%, relative to an existing set-point HVAC control system.

2. Materials and methods

2.1. Design of a wearable temperature sensor

The wearable temperature sensor consists of three thermistors, a BLE SoC, a coil antenna, a power management circuit and a 3.7 V lithium polymer battery. A 3 V constant voltage source was applied to each 10 kΩ resistor, and they were serially connected to each thermistor. Subsequently, the voltage across the thermistor was used to convert the measured analog voltage signal to digital values in the BLE-SoC and communicate with the external BLE module. In the meantime, the coil antenna was connected with the integrated 100 mAh battery through a full-wave voltage doubler circuit for wireless charging. We used Feig Dynamic Antenna Tuner (FEIG ELECTRONIC®) for wireless charging of the device to automatically match the impedance of the transmitter to the 13.56 MHz standard frequency. To test the charging performance of the wearable device, a 5 W radiofrequency signal was applied on the wearable device by placing it on top of the transmitter.

2.2. Fabrication of a soft wearable temperature sensor

Flexible printed circuit board (FPCB) for soft wearable temperature sensors was fabricated through the photolithography process. Copper was deposited and patterned on polyimide (PI) substrate and then insulating PI layer was stacked on the patterned copper traces. Another copper trace layer was patterned on the stacked PI layer. A total of four individual constituent layers of copper traces were patterned in the same way. Among the four copper layers of the FPCB, the top and the bottom layers (35 μm in thickness each) were patterned to create traces that served as interconnects of the circuit, while the two middle layers (18 μm in thickness each) were used to make coil patterns (14 turns) which served as an antenna for wireless charging. Electronic components (e.g., thermistors, resistors, capacitors, diodes, BLE-SoC, and battery) were mounted on copper electrodes on the top and bottom of the fabricated FPCB using a low-temperature solder paste (T5, SMDLTLFP10T5, Chip Quik). After ensuring that each component was mounted on their proper location, the device was placed inside a reflow oven (AS-5060, SMTmax) with peak temperature of 215 °C for 90 s. Then, the device was encapsulated with a soft, adhesive silicone (Silbione RT Gel 4717, Bluestar Silicones; 2 mm in thickness) using polylactic acid (PLA) molds fabricated using a 3D printer (3DP-310 F, CUBICON).

2.3. Adhesion strength test

To compare the adhesion strength of various biocompatible adhesive materials, a standard vertical peel measurement test (ASTM Volume 15.06, 2021) was employed for each type of material. Two mixing ratios (i.e., 10:1 and 15:1) were used for the following biocompatible adhesive materials – that is, Silbione 4717 (Bluestar Silicones®), Ecoflex gel (Smooth-On®), Ecoflex 0030 (Smooth-On®), Polydimethylsiloxane (PDMS, Dow corning®). Each test sample (2.5 cm (l) × 2.5 cm (w) × 1.0 mm (t)) was placed on the skin of the flexor muscle and peeled-off vertically (90° angle) using a force gauge equipment (Mark-10). The adhesion strength of each material was calculated by dividing the measured force by the contact area between the test sample and the skin. Note that l, w, and t denote length, width, and thickness of the test samples.

2.4. Water vapor transmission rate study

The water vapor transmission rate values for Silbione 4717 and commercial wristband (Urethane) were measured based on ASTM E96 (ASTM standard, 1989). Briefly, granulated dry cobalt chloride (Drierite, W.A. Hammond Drierite Co., LTD) was poured in the flasks (125 mL). Then, each test sample (i.e., Silbione 4717: thickness of 0.5 mm, 1 mm, 2 mm; urethane-based wristband: thickness of 1 mm) was used to seal the flask appropriately. The total weight change of each flask was measured for five days in a controlled environment (23 °C, 50% humidity).

2.5. Characterization of temperature sensors

The resistance changes of the thermistors were calibrated for the temperature measurements using a commercial infrared (IR) camera (A655sc, FLIR®) with varying temperature conditions using a hot plate (MSH-50D, DAIHAN-brand). Then, the accuracy of the calibrated temperature sensors, which were on top of the hotplate, was validated by comparing the reading with the one from the IR camera while changing the temperature of the hot plate. To determine the reliability of temperature sensing during mechanical distortions, various semicircle-shaped plastic models with different radius of curvature and mechanical stretcher were used to simulate the bending and stretching conditions of the device during use.

2.6. Mechanical modeling and FEA

To verify the mechanical robustness of the wearable device for long-term use in daily life, a commercial finite element analysis (FEA) software (Abaqus, Dassault Systèmes) was used. A 3D model of the wearable skin temperature sensor (four-layered flexible printed circuit board with encapsulating polymer (Silbione 4717) was created. To verify the mechanical robustness of the device in terms of stretching, bending, and twisting conditions, the following parameters were used for simulation: stretching of 20%; bending with radius of curvature of 10 mm; and twisting to 180°, respectively.

2.7. Algorithms for thermal comfort prediction

To evaluate thermal comfort prediction models, five-fold cross-validations was used for various regression and classification models with following implementations. For random forest model, 106 trees were used for training (minimum samples split was 2, maximum depth was 46, and other parameters followed default condition). Also, linear regression model, logistic regression model, random forest regression, support vector machine, ridge classifier, logistic discriminant analysis, support vector classifier (linear kernel, other conditions are default), gradient boosting machine classifier, and k-nearest neighbor classifier were implemented using python 3.9 with scikit-learn 1.0.2 and default parameters were used unless specified.

2.8. HVAC power consumption measurement

To determine the HVAC power consumption, a measurement system (SEM3000, KORINS) was used, which is composed of a plug-in type sensor and a receiver. The plug-in type sensor of the measuring device was connected to the air conditioning unit, and the power consumption of the air conditioning unit was wirelessly transmitted to the receiver. The receiver was connected to the internet and the transmitted power consumption (kWh) was recorded in the internet server every 1 minute. The total power consumption could be analyzed by simply summing up the power consumption every minute.

2.9. HRV measurement and analysis

To measure the individual heart rate variability (HRV) for each thermal condition (cool discomfort, comfort, warm discomfort), an electrocardiogram (ECG) was monitored using a three-lead wireless heart rate recording device (BioRadio, Great lakes Neurotechnologies®) with its software (BioCapture, Great lakes Neurotechnologies®). For every human participant, each of the three foam snap electrodes was placed as follows: one on the left arm, another one on the right arm, and the last one on the right leg (for ground). Each signal was recorded using the recording device with shielded lead cables. Then, the signal was transmitted to a computer using the Bluetooth communication. The measured ECG signal was analyzed by a customized software (MATLAB, MathWorks®). The R-R interval was analyzed by calculating the successive differences of the R-peaks with sampling frequency of 2 kHz, and the HRV values could be determined by calculating the successive differences of R-R intervals.

2.10. Experiments on human subjects

All experiments on human were performed under the approval from Institutional Review Board at Korea Advanced Institute of Science and Technology (protocol number: KH 2018-35), and all the volunteer subjects received informed consent.

3. Results and discussion

3.1. Wearable thermal preference prediction platform for real-time HIL control of the HVAC system

Fig. 1a and b respectively show a conceptual illustration and an operation block diagram of a wearable thermal preference prediction platform for real-time HIL control of the HVAC system, which enables personalized thermal comfort management and building energy savings. The platform consists of a soft wearable three-point temperature sensor, external sensors measuring the room temperature and humidity, an AI model that provides thermal comfort prediction, and an HVAC system. The wearable temperature sensor captures the thermal condition of an occupant, and the external temperature and humidity sensors monitor the ambient thermal conditions, which serve as a feedforward signal for the thermoregulation system of the human body (Charkoudian, 2003; Romanovsky, 2014). Additionally, the system collects information on age, sex (Kingma and van Marken Lichtenbelt, 2015), and clothing insulation (American Society of Heating, 2005) through a one-time user survey via a smartphone application (created using the MIT App Inventor, Massachusetts Institute of Technology; Fig. S1). All this information is transmitted wirelessly to a cloud server through Bluetooth communication, where the AI model makes real-time prediction of the thermal comfort status of the occupant and provides closed-loop control of the HVAC system to optimize the room temperature for maximal thermal comfort of the occupants.

The wearable temperature sensor plays a pivotal role for continuous, real-time monitoring of the thermophysiological condition of an individual. Reportedly, the wrist is the most responsive body part reflecting one's thermal status (Choi and Loftness, 2012). For this reason, many recent studies have used the wrist as the point of measurement to monitor one's thermal comfort (Aryal and Becerik-Gerber, 2019; Deng and Chen, 2020; Jung et al., 2019; Li et al., 2021; Liu et al., 2019; Nazarian et al., 2021; Park and Park, 2022; Sim et al., 2016). Further, a previous study (Sim et al., 2016) revealed that the three-point temperature measurement from the upper wrist, the radial artery, and the ulnar artery leads to improved thermal comfort prediction compared to single-point temperature measurement from the wrist. We created a wristband-like soft device that can be laminated conformally on the skin following the curvature of wrist for three-point temperature measurement (Fig. 1c–e). A different subject's skin temperatures at correct locations can be measured after checking one's pulse on the radial artery and ulnar artery locations as shown in Fig. S2. For the upper wrist region, one can simply place the sensor at the center of upper wrist. Fig. 1c shows an exploded-view schematic diagram of the device, which includes three thermistors (NCP15XH103F03 R C, Murata Electronics), a Bluetooth Low Energy System-on-Chip (BLE SoC, EYSHSNZWZ, Taiyo Yuden), a power management circuit with a coil antenna (18 μm-thick copper traces, 14 turns), and a rechargeable lithium polymer battery (100 mAh, LiPol Battery Co.) in a compact, flexible, and stretchable printed circuit (Figs. S3 and S4) encapsulated with an adhesive, air-permeable soft silicone (Silbione RT Gel 4717, Elkem Silicones; 2 mm thickness; Figs. S5 and S6). The thermistors (temperature coefficient of resistance; $-3.8\%\cdot{}^{\circ}C^{-1}$), which change their resistance according to the temperature, are used as temperature sensors. The temperature sensing circuit provides temperature-dependent voltage values to the analog–digital converter (ADC) unit of the BLE SoC to transmit digitalized data to a cloud server via Bluetooth communication. The encapsulating silicone of the device offers not only high adhesion force (1.5 kPa) that enables intimate contact of sensors to the skin for stable temperature monitoring (Fig. 1e and Fig. S5), but also a sufficiently high water vapor transmission rate (WVTR = $0.417\ g\cdot m^{-2}\cdot day^{-1}$; Fig. S6), thereby facilitating evaporation of sweat necessary for thermal regulation of the skin. The optical and SEM images showing the cross-section of the device before and after the water evaporation test (Fig. S7) shows that the morphologies remain the same due to its high water vapor

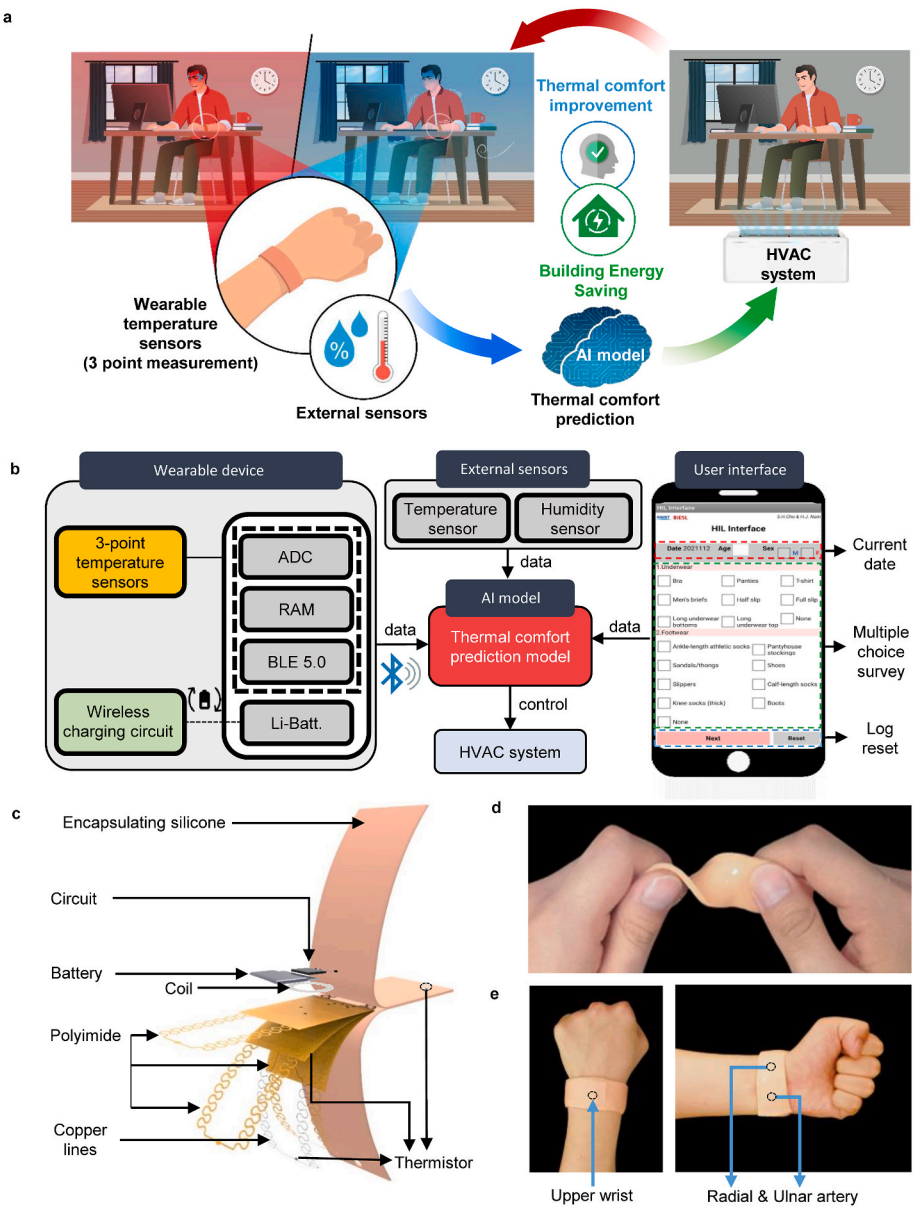

Fig. 1. Overview of the wearable thermal preference prediction platform for real-time human-in-the-loop control of the Heating, Ventilation, and Air Conditioning (HVAC) system for personalized thermal comfort management and building energy savings. a) Conceptual illustration of the overall system. An occupant's thermal comfort level is predicted by an AI model based on environmental data and his/her skin temperature measured by a wearable sensor, and is used to make closed-loop control of the HVAC system. b) Block diagram showing the overall system operation. c) Exploded-view schematic diagram of the soft wearable sensor, consisting of three thermistors, a Bluetooth Low Energy System-on-Chip (BLE SoC), a coil antenna, a power management circuit, and a battery. d) Photograph of the wearable temperature sensor highlighting its high deformability. e) Photograph of the same device attached on the wrist such that each thermistor accesses the upper wrist, radial artery, and ulnar artery.

permeability allowing evaporation of water instead of absorbing it in its material. This feature minimizes the influence of the wearable device on the skin temperature, allowing accurate temperature measurement that reflects bodily thermal comfort status. This is a clear advantage over commercial wristband temperature sensors, which are based on urethane (WVTR = ~0 $g \cdot m^{-2} \cdot day^{-1}$; Fig. S6). The wearable temperature sensor is elastic and highly deformable due to its interconnect design with a filamentary serpentine structure. Therefore, it allows facile adjustment of thermistor positions on the skin regardless of the size of the wrist (e.g., male versus female) to precisely access the upper wrist point and radial and ulnar arteries for three-point measurement (Fig. 1e). The wearable sensor can operate for over 12 h with a sampling rate of 1/30 Hz after 30 min wireless charging (power transmission frequency: 13.56 MHz) (Fig. S8), supporting sufficiently long and continuous monitoring of an individual's thermal condition. Details on the circuit design and fabrication process of the wearable sensor can be found in the Materials and methods section.

3.2. *Mechanical and thermal characterization of the wearable temperature sensor*

Wearable temperature sensors should maintain mechanical robustness and electrical reliability for long-term use in daily life. To ensure the mechanical robustness of the wearable device, experimental and analytical studies were conducted for three different scenarios (i.e., stretching, bending, and twisting), as shown in Fig. 2a. A finite element analysis revealed that the circuit design with serpentine interconnects allows stretching over 20%, bending with a radius of curvature of 10 mm, and twisting of 180° with only maximum principle strain of 0.7%, 2%, and 0.9% in the metal (Cu) traces, respectively. Considering that the fracture strain of Cu is much higher (20–40% (Carreker and Hibbard, 1953)), the results verify the robust and compliant nature of the device that can adapt to various deformations required for integration onto the curvilinear, dynamically changing surface of the skin. Further, it makes the device universally useable for people with different wrist sizes by allowing facile placement of the three sensors on the correct measurement points (upper wrist, radial artery, and ulnar artery) through elastic adaptation.

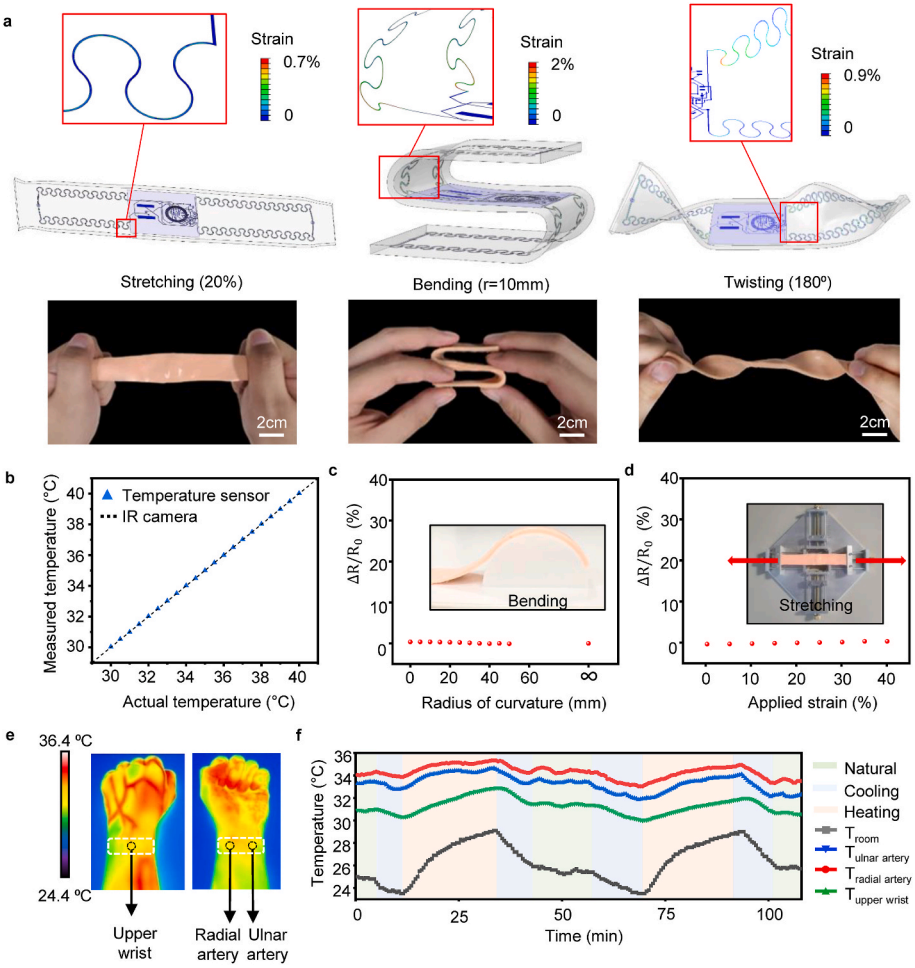

Fig. 2. Mechanical and thermal characterization of the wearable temperature sensor. a) Finite element modeling of the wearable sensor for stretching (20%), bending (10 mm radius of curvature), and twisting (180°) deformation (top) and the corresponding optical image of the device (bottom). b) Plot showing high accuracy of the wearable temperature sensor comparable with the performance of an infrared (IR) camera. c) Relative resistance changes of the wearable temperature sensor as a function of bending radius. d) Relative resistance changes of the same device as a function of applied strain. e,f) Infrared images of the top and the bottom of the left arm showing the temperature sensing spots (i.e., upper wrist, radial artery, and ulnar artery) (e) and the correlation of skin temperatures with ambient temperature change (f). Green, blue, and orange backgrounds in the plot indicate that the room is in a natural, cooling, and heating condition, respectively. The gray, blue, red, and green lines indicate the temperature for the room, ulnar artery skin, radial artery skin, and the upper wrist skin, respectively.

The soft, elastic design of the wearable sensor leads to a reliable electrical operation, which is not affected by mechanical deformation such as bending and stretching. The integrated sensor provides highly accurate temperature sensing with resolution of 0.05 °C in the physiological temperature range (30–40 °C) (Chaudhuri et al., 2018b), which is comparable with the performance of an infrared (IR) camera (Fig. 2b). For wearable applications, it is important for the device to maintain the same, reliable sensing characteristic regardless of applied strain (Anastasova et al., 2017; Hattori et al., 2014; Jeong et al., 2014, 2013; Liu et al., 2016; Rodeheaver et al., 2021; Zhao et al., 2022). In this device architecture, since the sensing elements (i.e., thermistors) are connected with metal interconnects in series, any resistance change on the interconnects caused by the applied strain could hamper an accurate temperature measurement. Owing to the robust and stretchable design of the device, however, we could eliminate this potential issue, as demonstrated in Fig. 2c and d, which present negligible resistance changes with bending (radius of curvature from 0 to ∞) and stretching (up to 40%). These results ensure stable and reliable sensing ability for wearable body temperature measurement. Fig. 2e and f show the capability of the wearable sensor to provide real-time, continuous measurement of the bodily thermal response from the three key measurement points on the wrist (i.e., upper wrist, radial artery, ulnar artery). The wearable sensor can closely capture the temperature changes of the three wrist points (Fig. 2e) over time, reflecting the body's response to the change of the room temperature controlled by a commercial heater and an air conditioner. The temperature value predominance as well as the temperature difference between each skin location change over time, indicating that the three-point temperature measurement can contribute to improving the thermal comfort prediction (Fig. 2f and Fig. S9). Therefore, we subsequently used the sensor to collect the thermophysiological data necessary to make a real-time prediction of an occupant's thermal comfort using the AI model.

3.3. Performance of machine learning models for thermal comfort prediction

To develop the AI model for thermal comfort prediction, the environmental and skin physiological data of occupants (Table S1) were collected every 30 s in varying thermal environments. A total of 18 experiment sessions for seven subjects were conducted through the data collection scheme shown in Fig. 3a. The total dataset was divided into a 6:2:2 ratio for training, testing, and validation sets for hyper parameter tuning of the model using Bayesian optimization. Using five-fold cross-validations, we tested various machine learning models and compared the thermal comfort prediction performance of different AI models (Fig. 3b) including regression models (linear regression, logistic regression, random forest regression, support vector machine regression) and classification models (random forest classifier, ridge classifier, logistic discriminant analysis, support vector classifier, gradient boosting machine classifier, and k-nearest neighbor classifier). Random forest classifier, an ensemble learning method that uses a collection of weak learners based on decision trees, showed the best performance among the machine learning models. A representative model of random forest is illustrated in Fig. 3c (Breiman, 2001). A wide variety of studies based on machine learning have been successfully carried out using the random forest algorithm (Aryal and Becerik-Gerber, 2020; Chaudhuri et al., 2018b), consistent with our results. Fig. 3d summarizes the prediction performance of the applied random forest classifier by constructing a

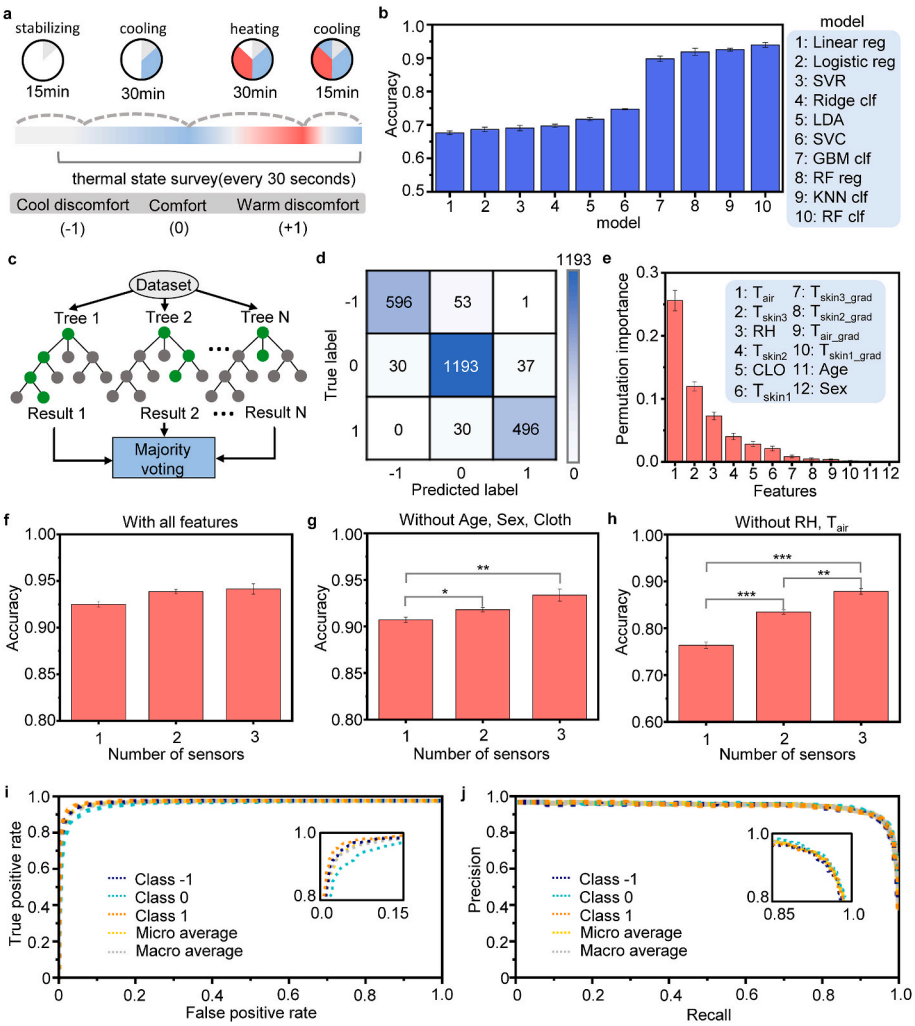

Fig. 3. Performance of machine learning models for thermal comfort prediction. a) Experimental procedure for collecting the thermal state by changing the thermal environment in the sequence of 15 min stabilization, 30 min cooling, 30 min heating, and 30 min cooling. The thermal comfort questionnaire includes three thermal states: cool discomfort, comfort, and warm discomfort. b) Comparison of accuracy of machine learning models including linear regression, logistic regression, Support Vector Machine (SVR), Ridge classifier, Logistic Discriminant Analysis (LDA), Support Vector Classifier (SVC), Gradient Boosting Machine (GBM) classifier, Random Forest (RF) regression, K-Nearest Neighbor (KNN) classifier, and RF classifier. c) Schematic diagram of the random forest classifier. d) Confusion matrix of the model with a total of 3045 data for the thermal comfort value with cool discomfort (−1), comfort (0), and warm discomfort (+1). e) Permutation importance of the features using the RF classifier. The abbreviated expressions for features in the blue box are defined in (f). f) Thermal comfort prediction accuracy according to the number of sensors when using all features of air temperature (T_{air}), upper wrist skin temperature (T_{skin3}), relative humidity (RH), ulnar artery skin temperature (T_{skin2}), radial artery skin temperature (T_{skin1}), upper wrist skin temperature gradient (T_{skin3_grad}), ulnar artery skin temperature gradient (T_{skin2_grad}), air temperature gradient (T_{air_grad}), radial artery skin temperature gradient (T_{skin1_grad}), clothing factor (CLO), sex, and age. g, h) Accuracy of thermal comfort prediction when using all features except age, sex, clothing factor (g), or all features except RH and T_{air} (h). (*p-value<0.05, * *p-value<0.01, * * *p-value<0.001). i,j) Receiver operating characteristic curve (i) and precision-recall curve (j) of the RF classifier. The insets show magnified views of the upper left and the upper right part of the curves in (i) and (j), respectively.

confusion matrix for each class. The prediction accuracies for each class of thermal comfort were 91.7% (cold discomfort; class −1), 94.7% (comfort state; class 0), and 94.3% (hot discomfort; class +1), respectively. To assess the importance of each feature and their contributions to the performance of the model, we used the permutation importance of input features to the trained random forest classifier, as shown in Fig. 3e. The permutation importance was analyzed by calculating the increment of prediction error when the target feature was randomly shuffled (Altmann et al., 2010). The results show that air temperature (T_{air}) has the largest permutation importance, followed by upper wrist skin temperature (T_{skin3}), relative humidity (RH), ulnar artery skin temperature (T_{skin2}), clothing factor (CLO), radial artery skin temperature (T_{skin1}), upper wrist skin temperature gradient (T_{skin3_grad}), ulnar artery skin temperature gradient (T_{skin2_grad}), air temperature gradient (T_{air_grad}), radial artery skin temperature gradient (T_{skin1_grad}), age, and sex. These results show that the feature importance of the sensing spots of the wrist varies, which is consistent with the results of a previous study (Sim et al., 2016) that reported varying accuracies for different sensing spots of the wrist.

Using the random forest model, accuracy comparisons were performed according to the number of skin temperature sensors in the wrist. A random forest model with 106 trees, a maximum depth of 46, minimum sample splits of two, and otherwise defaults of scikit-learn (Pedregosa et al., 2011) was used. The accuracy of the model (with all features) increased up to 93.9% (Fig. 3f) with the three-point measurements, which was similar to the best accuracy among the state-of-the-art thermal comfort prediction methods (Chaudhuri et al., 2020). Without information of age, sex, and clothing insulation variables, the wearable temperature sensor with three-point measurements exhibited a significant increase of accuracy of 2.9% (p-value <0.01), as compared with a single-point measurement (Fig. 3g). Additionally, without any external sensor information (RH and T_{air}), the wearable temperature sensor shows an even more significant increase of accuracy, 11.2% (p-value $<10^{-7}$), for three-point measurement relative to single-point measurement (Fig. 3h). This result shows that the multi-sensing strategy can be applied to improve the thermal comfort prediction performance. The custom wearable temperature sensor with three-point measurement can be a better choice for an efficient HIL-HVAC control system compared to the commercial wristband that uses single-point temperature measurement.

Additionally, since the overall accuracy does not take into account the different sizes of each class, we analyzed our model's performance using the receiver operating characteristic (ROC) (Fig. 3i) and precision recall (PR) curves (Fig. 3j) to show the prediction power of each class (Davis and Goadrich, 2006). The ROC curve assesses the trade-off between the true positive rate and the false positive rate of the trained model using different probability thresholds from 0 to 1. Similarly, the PR curve shows the trade-off between the true positive rate and the positive predictive value of the trained model. Both area under curve (AUC) values for ROC and PR were over 0.9 (Table S2) for each class, indicating that the AI thermal comfort prediction model can be applied to the HVAC control system with accurate thermal comfort prediction. However, this work focuses on investigating the thermal comfort prediction for occupants who underwent the thermal comfort experiments.

Therefore, the work that involved seven people in the experiment has limitation on building up a model that can perform for subject outside of the dataset, which is actually beyond the scope of this work.

3.4. Proof-of-concept demonstration of the HIL-HVAC control

Proof-of-demonstration experiments were held for the HIL-HVAC control system through monitoring of power consumption along with measurements of physiological changes of the body based on a heart rate variability (HRV) analysis. A block diagram of the overall system operation is shown in Fig. 4a. From the device, three-point wrist skin temperature values from the upper wrist, radial artery, and ulnar artery were obtained and these values were transmitted via Bluetooth low energy communication to a microcontroller interfaced with a computer. Using a smartphone application, the occupants input their age, sex, and clothing information, which were used as a clothing insulation factor. From the external sensors, air temperature and relative humidity values were measured. All these input values were automatically sent to the cloud server to feed the AI model as input in real-time. Based on these input variables and calculated three-point wrist skin temperature gradients, the AI model predicted the thermal comfort values. Finally, the corresponding HVAC control signal was calculated based on the thermal comfort value, and then sent to the HVAC system via IR communication. Every 30 s, for the hot discomfort condition (+1), the HVAC control system decreased the air temperature by 1 °C, whereas for the cold discomfort condition (−1), the HVAC control system increased the air temperature by 1 °C. To find the upper limit condition of the comfort state for energy-efficient operation, the setting temperature was increased by 1 °C for the comfort state (0) when the thermal comfort value changed from a cold discomfort state (−1) to the comfort state (0). Fig. 4b is a schematic diagram illustrating the experimental setup in a room and an optical image is shown in Fig. S10. With the real-time HIL controlling strategy, the HVAC system could be efficiently operated based on the individual thermal comfort prediction.

To validate our system's energy-saving performance, we measured and compared the power consumption for two different HVAC control strategies: HIL-based control and set-point control, as shown in Fig. 4c. For the set-point control, the target air temperature was set to 25 °C based on the thermal comfort zone from the ASHRAE standard 55 (Yoon et al., 2016), which is widely used for setting the temperature for building's HVAC systems. For each experiment, the power consumption and air temperature were monitored using a plug-type power meter (SEM3000, KORINS) and the data were updated to a cloud server. The total power consumption accumulated over time was compared with the HVAC system's power consumption (Fig. 4d). By using the HIL-based control system, the total power consumption was reduced by 20% compared to the set-point control (i.e., 131 kWh power consumption for set-point control vs. 105 kWh for the HIL-based control for a 6-h operation).

Physiological responses to thermal environments have also been shown to be correlated with thermal comfort (Nkurikiyeyezu et al., 2018; Shin, 2016). HRV is widely used to analyze the response of the autonomic nervous system to changes in the internal and external environment by observing small changes in the time interval between successive heartbeats (Le et al., 2022; Shaffer and Ginsberg, 2017). To validate the thermal comfort assessment, we analyzed HRV within the HIL-HVAC control system environment by measuring the electrocardiogram (ECG). ECG signals were measured with three-lead electrodes which were place on the left arm, right arm, and right leg (ground), as shown in Fig. S11, and the collected data was sent to a computer via Bluetooth communication. Fig. 4e shows the individual HRV range of each thermal comfort value. The average HRV value decreased from 33.8 ms to 16.5 ms as the thermal comfort changed from −1 to +1. This result is consistent with the ones of the previous studies (Nkurikiyeyezu et al., 2018; Shin, 2016; Wang et al., 2022), which reported that the average HRV increases in the cool discomfort condition, while decreases

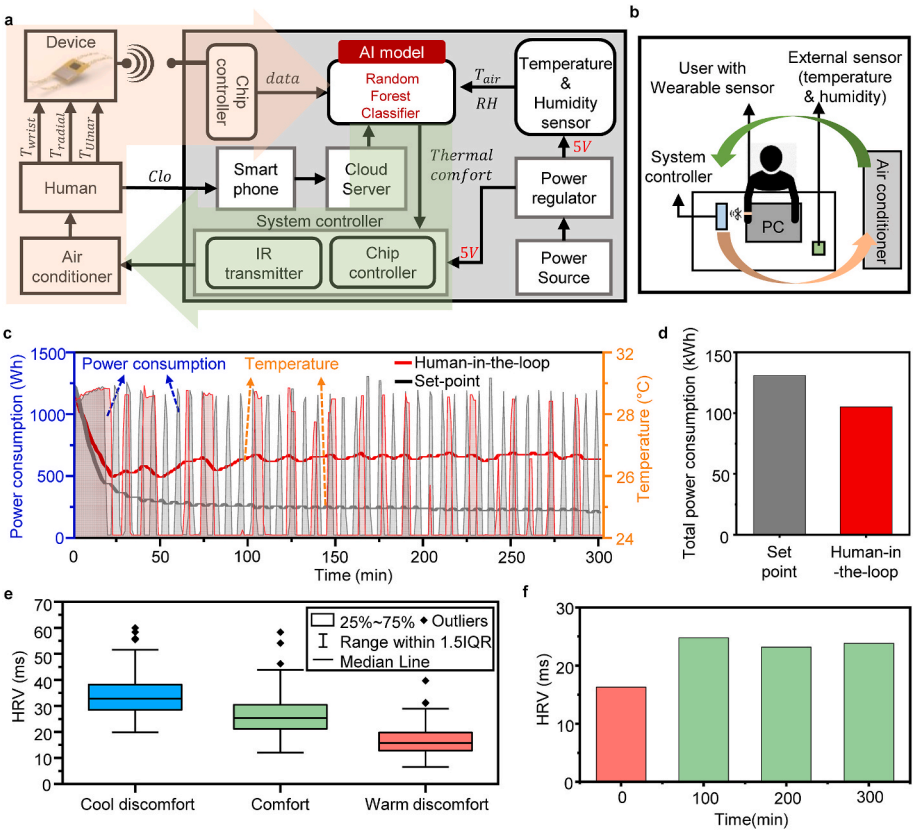

Fig. 4. Proof-of-concept demonstration of human-in-the-loop (HIL) HVAC control for an occupant's thermal comfort management and building's energy savings. a) Block diagram of the overall system operation for HIL-HVAC control. b) Schematic diagram illustrating the experimental setup in a room. c) Plot comparing power consumption of the HVAC system and room temperature changes made by two different approaches: HIL-based (red) vs. set-point-based HVAC control (gray; set temperature = 25 °C). Blue y-axis and arrows indicate power consumption, and orange y-axis and arrows indicate room temperature. d) Total power consumption of the set-point (gray) and the HIL-based control (red), highlighting high energy-efficiency of the HIL-based approach. e) An occupant's heart rate variability (HRV) range for different thermal comfort conditions (i.e., cool discomfort, comfort, and warm discomfort). f) Measurement of the occupant's HRV during HIL-based HVAC operation in (c). The data show that the occupant reaches a thermally comfortable state in about 100 min and remains in this state.

in the warm discomfort condition, relative to the one in the thermally comfortable state. Based on this result, we used the measured HRV as a thermal comfort indicator to verify the performance of our thermal comfort prediction system. Fig. 4f compares the HRV changes over time under machine learning-based HIL-HVAC control. For the warm discomfort state at time 0 in Fig. 4c, the measured HRV value was in the range of the individual HRV values for a warm discomfort state in Fig. 4e. As the HIL-HVAC control system regulates the temperature of the room, the occupant had reached a more comfortable state, as signified by the measured HRV values at 100, 200, and 300 min (Fig. 4e). The results verify that the system predicts the subject's relevant thermal comfort. The proof-of-demonstration confirms that the real-time HIL-HVAC control system not only reduces energy consumption but also improves the thermal comfort of the occupants.

4. Conclusion

In summary, the AI-based HIL-HVAC control system interfaced with a skin-adhesive wearable sensor was shown to effectively and efficiently improve the thermal comfort of an occupant and reduce the building energy consumption by providing pertinent control inputs. The compliant wearable device equipped with a three-point temperature sensor allowed stable and accurate measurements despite mechanical distortions, which is indispensable for practical use in daily life. The thermal comfort prediction model based on the random forest algorithm exhibited the best prediction accuracy of 93.9%, which was enabled by a three-point wrist skin temperature measurement strategy. Compared to the set-point control, the AI-based HIL-HVAC control system could reduce building energy consumption by 20%. The monitored HRVs were consistent with the range of individual HRV values for the corresponding thermal comfort values, demonstrating that the real-time HIL-HVAC control system can reduce building energy consumption while offering optimal individual thermal comfort. In future work, the proposed HIL-HVAC system can be further improved by integration with additional physiological and environmental sensors such as a photoplethysmography sensor (Lee et al., 2022) with the compliant wearable platform for simultaneous monitoring of HRV. Moreover, since this system focuses on controlling the thermal comfort of an individual occupant, in order to ensure wider applicability, statistical optimization approach (Gao et al., 2020; Li et al., 2021) would need to be applied to maximize the number of occupants feeling thermal comfort. Lastly, to enable a system that can satisfy multiple occupants, additional hardware which can control each occupant's thermal environment needs to be developed and integrated in the future.

CRediT authorship contribution statement

Seonghun Cho: Methodology, Software, Investigation, Visualization, Writing – original draft. **Hong Jae Nam:** Methodology, Software, Visualization. **Chuanqi Shi:** Methodology, Visualization. **Choong Yeon Kim:** Methodology. **Sang-Hyuk Byun:** Methodology. **Karen-Christian Agno:** Methodology, Writing – review & editing. **Byung Chul Lee:** Methodology. **Jianliang Xiao:** Methodology. **Joo Yong Sim:** Methodology, Investigation, Writing – review & editing, Supervision. **Jae-Woong Jeong:** Conceptualization, Methodology, Investigation, Visualization, Writing – review & editing, Supervision.

Declaration of competing interest

The authors declare that they have no known competing financial interests or personal relationships that could have appeared to influence the work reported in this paper.

Data availability

Data will be made available on request.

Acknowledgements

This work was supported by the Basic Science Research Program through the National Research Foundation of Korea (NRF) funded by the Ministry of Science and ICT (NRF-2022M3E5E9017759, NRF-2021R1A2C4001483, and NRF-2022R1C1C1008508).

Appendix A. Supplementary data

Supplementary data to this article can be found online at https://doi.org/10.1016/j.bios.2022.115018.

References

Akimoto, T., Tanabe, S., Yanai, T., Sasaki, M., 2010. Thermal comfort and productivity - evaluation of workplace environment in a task conditioned office. Build. Environ. 45, 45–50. https://doi.org/10.1016/j.buildenv.2009.06.022.

Altmann, A., Toloşi, L., Sander, O., Lengauer, T., 2010. Permutation importance: a corrected feature importance measure. Bioinformatics 26, 1340–1347. https://doi.org/10.1093/bioinformatics/btq134.

American Society of Heating, 2005. Refrigerating and Air-Conditioning Engineers, 2005 ASHRAE handbook: fundamentals. ASHRAE, Atlanta, GA.

Anastasova, S., Crewther, B., Bembnowicz, P., Curto, V., Ip, H.M., Rosa, B., Yang, G.-Z., 2017. A wearable multisensing patch for continuous sweat monitoring. Biosensors and Bioelectronics, Special Issue Selected papers from the 26th Anniversary World Congress on Biosensors (Part II) 93, 139–145. https://doi.org/10.1016/j.bios.2016.09.038.

Aryal, A., Becerik-Gerber, B., 2019. A comparative study of predicting individual thermal sensation and satisfaction using wrist-worn temperature sensor, thermal camera and ambient temperature sensor. Build. Environ. 160, 106223 https://doi.org/10.1016/j.buildenv.2019.106223.

Aryal, A., Becerik-Gerber, B., 2020. Thermal comfort modeling when personalized comfort systems are in use: Comparison of sensing and learning methods. Build. Environ. 185, 107316 https://doi.org/10.1016/j.buildenv.2020.107316.

ASTM standard, 1989. Standard Test Methods for Water Vapor Transmission of Materials. Annual book of ASTM standards. ASTM, Philadelphia, PA.

ASTM Volume 15.06, 2021. Standard Test Method for 90 Degree Peel Resistance of Adhesives. ASTM, West Conshohocken, PA.

Breiman, L., 2001. Random forests. Mach. Learn. 45, 5–32. https://doi.org/10.1023/A:1010933404324.

Carreker, R.P., Hibbard, W.R., 1953. Tensile deformation of high-purity copper as a function of temperature, strain rate, and grain size. Acta Metall. 1, 654–663. https://doi.org/10.1016/0001-6160(53)90022-4.

Charkoudian, N., 2003. Skin blood flow in adult human thermoregulation: how it works, when it does not, and why. Mayo Clin. Proc. 78, 603–612. https://doi.org/10.4065/78.5.603.

Chaudhuri, T., Zhai, D., Soh, Y.C., Li, H., Xie, L., 2018a. Thermal comfort prediction using normalized skin temperature in a uniform built environment. Energy Build. 159, 426–440. https://doi.org/10.1016/j.enbuild.2017.10.098.

Chaudhuri, T., Zhai, D., Soh, Y.C., Li, H., Xie, L., 2018b. Random forest based thermal comfort prediction from gender-specific physiological parameters using wearable sensing technology. Energy Build. 166, 391–406. https://doi.org/10.1016/j.enbuild.2018.02.035.

Chaudhuri, T., Soh, Y.C., Li, H., Xie, L., 2020. Machine learning driven personal comfort prediction by wearable sensing of pulse rate and skin temperature. Build. Environ. 170, 106615 https://doi.org/10.1016/j.buildenv.2019.106615.

Choi, J.-H., Loftness, V., 2012. Investigation of human body skin temperatures as a bio-signal to indicate overall thermal sensations. Build. Environ. 58, 258–269. https://doi.org/10.1016/j.buildenv.2012.07.003.

Collinge, W.O., Landis, A.E., Jones, A.K., Schaefer, L.A., Bilec, M.M., 2014. Productivity metrics in dynamic LCA for whole buildings: using a post-occupancy evaluation of energy and indoor environmental quality tradeoffs. Build. Environ. 82, 339–348. https://doi.org/10.1016/j.buildenv.2014.08.032.

Cosma, A.C., Simha, R., 2019. Machine learning method for real-time non-invasive prediction of individual thermal preference in transient conditions. Build. Environ. 148, 372–383. https://doi.org/10.1016/j.buildenv.2018.11.017.

Damassa, T., 2014. Climate analysis indicators tool (CAIT). In: Michalos, A.C. (Ed.), Encyclopedia of Quality of Life and Well-Being Research. Springer Netherlands, Dordrecht, pp. 949–951. https://doi.org/10.1007/978-94-007-0753-5_403.

Davis, J., Goadrich, M., 2006. The relationship between Precision-Recall and ROC curves. Proceedings of the 23rd international conference on Machine learning (ICML '06) 233–240. https://doi.org/10.1145/1143844.1143874.

Deng, Z., Chen, Q., 2020. Development and validation of a smart HVAC control system for multi-occupant offices by using occupants' physiological signals from wristband. Energy Build. 214, 109872 https://doi.org/10.1016/j.enbuild.2020.109872.

Fang, Y., Chen, G., Bick, M., Chen, J., 2021. Smart textiles for personalized thermoregulation. Chem. Soc. Rev. 50, 9357–9374. https://doi.org/10.1039/D1CS00003A.

Gao, G., Li, J., Wen, Y., 2020. DeepComfort: energy-efficient thermal comfort control in buildings via reinforcement learning. IEEE Internet Things J. 7, 8472–8484. https://doi.org/10.1109/JIOT.2020.2992117.

Han, J., Bae, J., Jang, J., Baek, J., Leigh, S.-B., 2019. The derivation of cooling set-point temperature in an HVAC system, considering mean radiant temperature. Sustainability 11, 5417. https://doi.org/10.3390/su11195417.

Hattori, Y., Falgout, L., Lee, W., Jung, S.-Y., Poon, E., Lee, J.W., Na, I., Geisler, A., Sadhwani, D., Zhang, Y., Su, Y., Wang, X., Liu, Z., Xia, J., Cheng, H., Webb, R.C., Bonifas, A.P., Won, P., Jeong, J.-W., Jang, K.-I., Song, Y.M., Nardone, B., Nodzenski, M., Fan, J.A., Huang, Y., West, D.P., Paller, A.S., Alam, M., Yeo, W.-H., Rogers, J.A., 2014. Multifunctional skin-like electronics for quantitative, clinical monitoring of cutaneous wound healing. Advanced Healthcare Materials 3, 1597–1607. https://doi.org/10.1002/adhm.201400073.

Hu, R., Liu, Y., Shin, S., Huang, S., Ren, X., Shu, W., Cheng, J., Tao, G., Xu, W., Chen, R., Luo, X., 2020. Emerging materials and strategies for personal thermal management. Adv. Energy Mater. 10, 1903921 https://doi.org/10.1002/aenm.201903921.

Jeong, J.-W., Yeo, W.-H., Akhtar, A., Norton, J.J.S., Kwack, Y.-J., Li, S., Jung, S.-Y., Su, Y., Lee, W., Xia, J., Cheng, H., Huang, Y., Choi, W.-S., Bretl, T., Rogers, J.A., 2013. Materials and optimized designs for human-machine interfaces via epidermal electronics. Adv. Mater. 25, 6839–6846. https://doi.org/10.1002/adma.201301921.

Jeong, J.-W., Kim, M.K., Cheng, H., Yeo, W.-H., Huang, X., Liu, Y., Zhang, Y., Huang, Y., Rogers, J.A., 2014. Capacitive epidermal electronics for electrically safe, long-term electrophysiological measurements. Advanced Healthcare Materials 3, 642–648. https://doi.org/10.1002/adhm.201300334.

Jung, W., Jazizadeh, F., Diller, T.E., 2019. Heat flux sensing for machine-learning-based personal thermal comfort modeling. Sensors 19, 3691. https://doi.org/10.3390/s19173691.

Katić, K., Li, R., Zeiler, W., 2020. Machine learning algorithms applied to a prediction of personal overall thermal comfort using skin temperatures and occupants' heating behavior. Appl. Ergon. 85, 103078 https://doi.org/10.1016/j.apergo.2020.103078.

Kingma, B., van Marken Lichtenbelt, W., 2015. Energy consumption in buildings and female thermal demand. Nat. Clim. Change 5, 1054–1056. https://doi.org/10.1038/nclimate2741.

Kramer, T., Garcia-Hansen, V., Nik, S.O.V.M., Chen, D., 2021. A Machine Learning approach to enhance indoor thermal comfort in a changing climate. J. Phys.: Conf. Ser. 2042, 012070 https://doi.org/10.1088/1742-6596/2042/1/012070.

Le, T., Zhang, J., Nguyen, A.H., Trigo Torres, R.S., Vo, K., Dutt, N., Lee, J., Ding, Y., Xu, X., Lau, M.P.H., Cao, H., 2022. A novel wireless ECG system for prolonged monitoring of multiple zebrafish for heart disease and drug screening studies. Biosens. Bioelectron. 197, 113808 https://doi.org/10.1016/j.bios.2021.113808.

Lee, G.H., Kang, H., Chung, J.W., Lee, Y., Yoo, H., Jeong, S., Cho, H., Kim, J.-Y., Kang, S.-G., Jung, J.Y., Hahm, S.G., Lee, J., Jeong, I.-J., Park, M., Park, G., Yun, I.H., Kim, J. Y., Hong, Y., Yun, Y., Kim, S.-H., Choi, B.K., 2022. Stretchable PPG sensor with light polarization for physical activity–permissible monitoring. Sci. Adv. 8, eabm3622 https://doi.org/10.1126/sciadv.abm3622.

Li, W., Zhang, J., Zhao, T., Ren, J., 2021. Experimental study of an indoor temperature fuzzy control method for thermal comfort and energy saving using wristband device. Build. Environ. 187, 107432 https://doi.org/10.1016/j.buildenv.2020.107432.

Liu, Y., Norton, J.J.S., Qazi, R., Zou, Z., Ammann, K.R., Liu, H., Yan, L., Tran, P.L., Jang, K.-I., Lee, J.W., Zhang, D., Kilian, K.A., Jung, S.H., Bretl, T., Xiao, J., Slepian, M.J., Huang, Y., Jeong, J.-W., Rogers, J.A., 2016. Epidermal mechano-acoustic sensing electronics for cardiovascular diagnostics and human-machine interfaces. Sci. Adv. 2, e1601185 https://doi.org/10.1126/sciadv.1601185.

Liu, S., Schiavon, S., Das, H.P., Jin, M., Spanos, C.J., 2019. Personal thermal comfort models with wearable sensors. Build. Environ. 162, 106281 https://doi.org/10.1016/j.buildenv.2019.106281.

Mansi, S.A., Barone, G., Forzano, C., Pigliautile, I., Ferrara, M., Pisello, A.L., Arnesano, M., 2021. Measuring human physiological indices for thermal comfort assessment through wearable devices: a review. Measurement 183, 109872. https://doi.org/10.1016/j.measurement.2021.109872.

Morresi, N., Casaccia, S., Sorcinelli, M., Arnesano, M., Uriarte, A., Torrens-Galdiz, J.I., Revel, G.M., 2021. Sensing physiological and environmental quantities to measure human thermal comfort through machine learning techniques. IEEE Sensor. J. 21, 12322–12337. https://doi.org/10.1109/JSEN.2021.3064707.

Nalley, S., LaRose, A., 2021. Annual Energy Outlook 2021. U.S. Energy Information Administration, Washington, DC.

Nazarian, N., Liu, S., Kohler, M., Lee, J.K.W., Miller, C., Chow, W.T.L., Alhadad, S.B., Martilli, A., Quintana, M., Sunden, L., Norford, L.K., 2021. Project Coolbit: can your watch predict heat stress and thermal comfort sensation? Environ. Res. Lett. 16, 034031 https://doi.org/10.1088/1748-9326/abd130.

Nkurikiyeyezu, K.N., Suzuki, Y., Lopez, G.F., 2018. Heart rate variability as a predictive biomarker of thermal comfort. J. Ambient Intell. Hum. Comput. 9, 1465–1477. https://doi.org/10.1007/s12652-017-0567-4.

Park, H., Park, D.Y., 2022. Prediction of individual thermal comfort based on ensemble transfer learning method using wearable and environmental sensors. Build. Environ. 207, 108492 https://doi.org/10.1016/j.buildenv.2021.108492.

Pedregosa, F., Varoquaux, G., Gramfort, A., Michel, V., Thirion, B., Grisel, O., Blondel, M., Prettenhofer, P., Weiss, R., Dubourg, V., Vanderplas, J., Passos, A., Cournapeau, D., Brucher, M., Perrot, M., Duchesnay, É., 2011. Scikit-learn: machine learning in Python. J. Mach. Learn. Res. 12, 2825–2830.

Peng, Y., Cui, Y., 2020. Advanced textiles for personal thermal management and energy. Joule 4, 724–742. https://doi.org/10.1016/j.joule.2020.02.011.

Rodeheaver, N., Herbert, R., Kim, Y.-S., Mahmood, M., Kim, H., Jeong, J.-W., Yeo, W.-H., 2021. Strain-isolating materials and interfacial physics for soft wearable bioelectronics and wireless, motion artifact-controlled health monitoring. Adv. Funct. Mater. 31, 2104070 https://doi.org/10.1002/adfm.202104070.

Romanovsky, A.A., 2014. Skin temperature: its role in thermoregulation. Acta Physiol. 210, 498–507. https://doi.org/10.1111/apha.12231.

Shaffer, F., Ginsberg, J.P., 2017. An overview of heart rate variability metrics and norms. Front. Public Health 5, 258. https://doi.org/10.3389/fpubh.2017.00258.

Shin, H., 2016. Ambient temperature effect on pulse rate variability as an alternative to heart rate variability in young adult. J. Clin. Monit. Comput. 30, 939–948. https://doi.org/10.1007/s10877-015-9798-0.

Sim, S., Koh, M., Joo, K., Noh, S., Park, S., Kim, Y., Park, K., 2016. Estimation of thermal sensation based on wrist skin temperatures. Sensors 16, 420. https://doi.org/10.3390/s16040420.

Sim, J.K., Yoon, S., Cho, Y.-H., 2018. Wearable sweat rate sensors for human thermal comfort monitoring. Sci. Rep. 8, 1181. https://doi.org/10.1038/s41598-018-19239-8.

Valladares, W., Galindo, M., Gutiérrez, J., Wu, W.-C., Liao, K.-K., Liao, J.-C., Lu, K.-C., Wang, C.-C., 2019. Energy optimization associated with thermal comfort and indoor air control via a deep reinforcement learning algorithm. Build. Environ. 155, 105–117. https://doi.org/10.1016/j.buildenv.2019.03.038.

van Ruijven, B.J., De Cian, E., Sue Wing, I., 2019. Amplification of future energy demand growth due to climate change. Nat. Commun. 10, 2762. https://doi.org/10.1038/s41467-019-10399-3.

Wang, Z., Matsuhashi, R., Onodera, H., 2022. Towards wearable thermal comfort assessment framework by analysis of heart rate variability. Build. Environ. 223, 109504 https://doi.org/10.1016/j.buildenv.2022.109504.

Yoon, J.H., Baldick, R., Novoselac, A., 2016. Demand response control of residential HVAC loads based on dynamic electricity prices and economic analysis. Science and Technology for the Built Environment 22, 705–719. https://doi.org/10.1080/23744731.2016.1195659.

Zhao, T., Fu, Y., Sun, C., Zhao, X., Jiao, C., Du, A., Wang, Q., Mao, Y., Liu, B., 2022. Wearable biosensors for real-time sweat analysis and body motion capture based on stretchable fiber-based triboelectric nanogenerators. Biosens. Bioelectron. 205, 114115 https://doi.org/10.1016/j.bios.2022.114115.